HOKKAIDO UNIVERSITY

Title	Water-Resistant Pt Sites in Hydrophobic Mesopores Effective for Low-Temperature Ethylene Oxidation
Author(s)	Satter, Shazia S.; Hirayama, Jun; Kobayashi, Hirokazu et al.
Citation	ACS catalysis, 10(22), 13257-13268 https://doi.org/10.1021/acscatal.0c02816
Issue Date	2020-11-20
Doc URL	https://hdl.handle.net/2115/83304
Rights	This document is the Accepted Manuscript version of a Published Work that appeared in final form in ACS Catalysis, copyright c American Chemical Society after peer review and technical editing by the publisher. To access the final edited and published work see https://pubs.acs.org/doi/10.1021/acscatal.0c02816 .
Type	journal article
File Information	Manuscript_201013.pdf

Hokkaido University Collection of Scholarly and Academic Papers : HUSCAP

Water Resistant Pt Sites in Hydrophobic Mesopores Effective for Low Temperature Ethylene Oxidation

*Shazia S. Satter, Jun Hirayama, Hirokazu Kobayashi, Kiyotaka Nakajima, Atsushi Fukuoka**

Institute for Catalysis, Hokkaido University, Kita 21 Nishi 10, Kita-ku, Sapporo, Hokkaido 001-0021, Japan

KEYWORDS: Supported Pt catalyst, silica, ethylene oxidation, hydrophobicity, mesopores, *in-situ* FTIR

ABSTRACT

Structure-activity relationship of silica-supported Pt catalysts in aerobic oxidation of 50 ppm ethylene was studied at 0 °C with a fixed-bed flow reactor and *in-situ* characterization techniques using FTIR (Fourier-transform infrared) spectroscopy. The activity of all Pt catalysts examined here decreased by water molecules formed during stoichiometric oxidation of ethylene and became stable steadily. Mesoporous silica-supported Pt catalyst improved its steady-state activity after calcination of the support in air at 800 °C, whereas no such effect was observed for nonporous silica support. CO-pulse titration, H_2O adsorption measurements, ^{29}Si MAS NMR, and *in-situ*

FTIR along with catalytic activity studies revealed that the activity of mesoporous silica-supported Pt catalyst is higher than that of nonporous silica-supported ones, despite similar hydrophobicity and low Pt dispersion. *In-situ* characterization using CO as a molecular probe indicates that a part of Pt surface inside hydrophobic mesopores is not involved in hydrogen-bonding network among physisorbed water molecules and surface SiOH groups even after full hydration of catalyst surface, and bare Pt sites are expected to work more effectively for ethylene oxidation. Such "hydrophobic Pt surface" can only be formed on hydrophobic mesoporous silica support, which is probably due to Pt nanoparticles surrounded with hydrophobic siloxane network entirely. Unique environment derived from condensed siloxane network and restricted mesopores contributes largely to high activity of Pt nanoparticles for low temperature oxidation of trace ethylene.

INTRODUCTION

Ethylene causes excessive aging of fresh vegetables and fruits in the vegetable compartment of refrigerators even at low temperatures, which make these agricultural products difficult to keep the freshness in a long-term storage. Conventional cold chain system currently used for the storage and transportation of these fresh products requests a striking technology for the sustainable removal of trace ethylene at low temperatures. Although various methods such as non-selective oxidation with harsh and stoichiometric oxidant ($KMnO_4$),[1] physisorption using carbons and zeolites,[2] and catalytic oxidation using supported metal catalysts[3–8] have already been reported to remove trace ethylene, most of them cannot satisfy basic demands in terms of efficiency and long-term utility especially at low temperatures. Photocatalytic system is one successful example to sustainably remove trace ethylene in low temperature ranges; however, this system requires light

irradiation to form photoexcited holes and electrons available for the conversion of ethylene into acetaldehyde.[9] An effective approach to sustainable ethylene decomposition without light irradiation is the use of supported metal catalysts that can convert ethylene to CO_2 and H_2O. Co_3O_4-supported Au catalysts were reported to be active for the decomposition of trace ethylene at 0 °C and room temperature.[10–12] Recently, several heterogeneous catalysts using Pt, Ag, and Au as active sites have appeared to be effective for the aerobic oxidation of ethylene at low concentrations and low temperatures.[13–15] Despite their promising activities, structure-activity relationship to reveal the origin of their unique activities have not been studied so far, and researchers search for the strategy to maximize the activity of supported metal catalyst.

Supported Pt catalysts are widely recognized in academia and in industry as a series of durable heterogeneous catalysts for various redox reactions. Recently a mesoporous silica supported Pt catalyst was commercialized as an oxidation catalyst in 2015 in Japan for the ethylene removal at ppm level in household refrigerators. Pt nanoparticles supported on mesoporous silica can decompose ethylene to CO_2 and H_2O at 0 ºC[16] and used for a long time without loss of its activity once the ethylene reaction proceeds steadily.[17] Our group has studied ethylene oxidation (50 ppm) at 0 ºC over silica-supported Pt catalysts and found recently that in-situ formed water during stoichiometric ethylene oxidation largely decreases their activities.[17] The addition of water vapor to the catalyst column resulted in the drastic decrease in both conversion and carbon dioxide yield, while the activity was recovered gradually to original level in the dry conditions.[17] This phenomenon suggested that the catalytic activity depends on the concentration of physisorbed water on the surface of supported Pt catalyst.[18] Water molecules are mainly physisorbed on the surface of silica support; therefore, hydrophilic-hydrophobic property of silica support is one of crucial factors influencing the activity of Pt nanoparticles.

There are several methods for the modification of silica surface using organosilanes to control hydrophobic-hydrophilic property.[19,20] However, most of organic groups has low thermal stability to heat treatment, and thermal treatment in H_2 for the formation of active Pt nanoparticles causes decomposition of these organic groups. A simple calcination treatment was subjected to mesoporous and aerosol silicas to reduce the concentration of hydrophilic silanol, because the density of surface silanol groups directly affects the physisorption of water.[18] We have already demonstrated that the activity of mesoporous silica supported Pt catalyst is increased by the calcination of the support at high temperature. This improvement can be reasonably explained by the elimination of water molecules formed by complete ethylene oxidation from hydrophobic silica surface inside mesopores, which then accelerates the reaction by Pt nanoparticles. In this study, we attempt to identify the difference in catalytic behavior of Pt nanoparticles on nonporous and mesoporous silicas in ethylene oxidation. Nonporous silica (Aerosil-380, A380) and mesoporous silica (SBA-15) were used as supports for Pt nanoparticles, and hydrophilic-hydrophobic property of these supports was easily controlled by calcination treatment at various temperatures in air. Catalytic reactions in a fixed-bed flow reactor and *in-situ* characterization using Fourier-transform infrared (FTIR) spectroscopy were combined to clarify the difference among the catalysts.[21,22]

EXPERIMENTAL

Chemicals

Tetraethoxysilane (TEOS, 99.9%) was supplied from Kojundo Chemical Laboratory. Diamminedinitroplatinum(II) ($Pt(NH_3)_2(NO_2)_2$) solution purchased from Tanaka Kikinzoku Kogyo was used as a precursor to form Pt nanoparticles on silica supports. Pluronic 123 ($EO_{20}PO_{70}EO_{20}$, EO = ethylene oxide moiety, PO = propylene oxide moiety) was obtained from Sigma Aldrich. Hydrochloric acid (HCl, 36-38 wt%) was received from Fujifilm Wako Pure Chemical Corporation.

Catalyst Preparation

Mesoporous silica, SBA-15 was synthesized with the same procedures reported in the previous papers.[17,18] Two silica supports (SBA-15 and Aerosil 380 (A380)) were calcined at 800 °C in air to make them hydrophobic.[18] The silica support (1.00 g) was stirred in an aqueous solution (50 mL) containing $Pt(NH_3)_2(NO_2)_2$ (0.196 mL, 486 mM) at 30 °C for 3 h. After evaporation and subsequent drying at 50 °C under vacuum, the material was reduced at 400 °C for 2 h under a H_2 flow (30 mL min^{-1}), which gave the supported Pt catalyst (Pt loading of approximately 1.8 wt%). Pt/SBA-15 and Pt/A380 were synthesized from bare SBA-15 and A380, whereas calcined SBA-15 and A380 at 800 °C afforded Pt/SBA-15(800) and Pt/A380(800). Here values in parenthesis are denoted as calcination temperature of the support. After reduction all catalysts are exposed to air and handled under atmospheric conditions for further studies.

Characterization

Powder X-ray diffraction (XRD) patterns were measured using an X-ray diffractometer and Cu Kα radiation (Rigaku Ultima IV, 40 kV, 20 mA). N_2 adsorption−desorption experiments were conducted at −196 °C (MicrotracBEL BELSORP-Mini). Specific surface areas and pore diameters

were estimated with the Brunauer−Emmett−Teller (BET) equation and nonlocalized density functional theory (NLDFT), respectively. The samples were heated under vacuum at 120 °C for 4 h to remove physisorbed water. The average size of Pt nanoparticles was calculated by CO pulse titration (MicrotracBEL BELCAT II). After the reduction of the samples at 400 °C for 90 min under a H_2 flow (30 mL min^{-1}), CO chemisorption was performed at 50 °C under a continuous flow of CO (10%) in He. The size of the Pt nanoparticles was estimated from the Pt dispersion with the assumption on Pt:CO ratio to be 1:1. An ECA600 spectrometer (600 MHz, JEOL, Larmor frequency of 119 MHz) was used for the measurements of solid-state ^{29}Si magic angle spinning (MAS) nuclear magnetic resonance (NMR). The spin rate used to obtain the ^{29}Si MAS NMR spectra was 18 kHz. We expressed the frequency of the spectra with respect to an aqueous standard solution of sodium trimethylsilyl propionate. X-ray photoelectron spectroscopy (XPS) data were obtained using a JEOL JPC-9010MC instrument and a Mg Kα line at a pass energy of 20 eV. The position of C 1s (C 284.8 eV) was used for charge correction.

Catalytic Reaction

Scheme S1 shows a reaction system for catalytic oxidation of trace ethylene in a fixed-bed flow reactor (inner diameter, 4 mm) under atmospheric pressure. Catalyst (0.40 g, granular form, 355−500 μm in granule size) was pretreated at 150 °C for 2 h in the reaction tube under a He flow (40 mL min^{-1}). A gas mixture (C_2H_4, 50 ppm; O_2, 20%; N_2, 5%; He, balance) was fed to the catalyst bed at 0 °C with a space velocity (SV) of 1500 mL h^{-1} g^{-1}. The gases after the reaction were analyzed with online gas chromatography (Agilent 3000 A Micro GC) equipped with a thermal conductivity detector. Plot U (8 m) and molecular sieves 5A (10 m) columns were used to detect reactant (C_2H_4) and product (CO_2), in which the detection limit for C_2H_4 was calculated as 0.1 ppm. The ethylene conversion and CO_2 yield were calculated from

($[C_2H_4]_{in}-[C_2H_4]_{out}$)×100/$[C_2H_4]_{in}$ and $[CO_2]_{out}$×100/2$[C_2H_4]_{in}$, respectively, where $[C_2H_4]_{in}$, $[C_2H_4]_{out}$, and $[CO_2]_{out}$ correspond to initial C_2H_4 concentration, and C_2H_4 and CO_2 concentrations at the outlet of the reactor, respectively.

In-situ FTIR Measurements

CO adsorption was carried out to identify active Pt sites of Pt/SBA-15(800) and Pt/A380(800) in the presence or absence of physisorbed water. A pellet (30–40 mg) of the samples was placed in an IR cell connected with a gas flow system (Scheme S2). After heating at 150 °C for 2 h in a He flow (30 mL min^{-1}), the dried sample was exposed to a CO/He mixture (100 ppm) and then measured with FTIR (PerkinElmer Spectrum 100 with a MCT detector, resolution 4 cm^{-1}, integration 64 times) in certain intervals. The experiments were also conducted in the presence of water vapor. The dried pellet was treated with a He flow containing water vapor (10 mL $min^{-1}$of flow rate, approximately 0.95 vol.% of water content) and saturated with physisorbed water. The hydrated sample was contacted with a CO/H_2O/He mixture (10 mL min^{-1} of flow rate, 100 ppm of CO concentration, approximately 0.95 vol.% of water content) and recorded with FTIR at certain intervals.

In-situ FTIR studies combined with catalytic activity of ethylene oxidation were performed over hydrophilic catalysts (Pt/SBA-15 and Pt/A380) and hydrophobic catalysts (Pt/SBA-15(800) and Pt/A380(800)). The catalyst pellet (30−40 mg) in an IR cell was dehydrated at 150 °C for 2 h in a He flow (40 mL min^{-1}). A gas-mixture (50 ppm of C_2H_4, 20% of O_2, 5% of N_2, and He balance) was introduced to the cell at 28 °C under ambient pressure with a SV=15,000 mL h^{-1} g^{-1}, where ethylene concentrations in the inlet and outlet gas, and CO_2 concentration in the outlet gas were monitored by Agilent 3000 A Micro GC and used to calculate ethylene conversion and CO_2 yield. Water vapor was supplied to the reaction gas stream from 3 to 6 h using a home-made saturator

shown in Scheme S2. The temperature of the saturator was maintained at 6.5 °C to introduce certain amount of water vapor (0.95 vol.%) constantly to the gas mixture. After stopping the supply of water vapor, the reaction continued for additional 7 h. FTIR spectra were collected at certain intervals throughout the experiments.

DFT Calculations

Density functional theory (DFT) calculations were performed on the Gaussian 16 (Rev. A.03) software[23] at the unrestricted open-shell B3LYP/LanL2DZ (Pt)/6-31G(d,p) (C,H,O) level of theory, where orbitals were represented by pure spherical harmonics (5d, 7f).[24–28] For the vibration frequency calculations, anharmonic terms were included to correct the frequency without empirical scale factors. The Pt (111) surface was modeled by a Pt_{10} cluster having the same geometry as the bulk crystal, and Pt atoms other than the center one was fixed to preserve the (111) plane structure. The most stable spin multiplicity was 10 for this system, and this value was used in all the calculations. CO was coordinated to the central Pt atom, and up to three water molecules were arranged around. Atomic charge was analyzed with Charge Model 5 (CM5).[29]

RESULTS AND DISCUSSION

Structure and Catalysis of Pt/SBA-15(800)

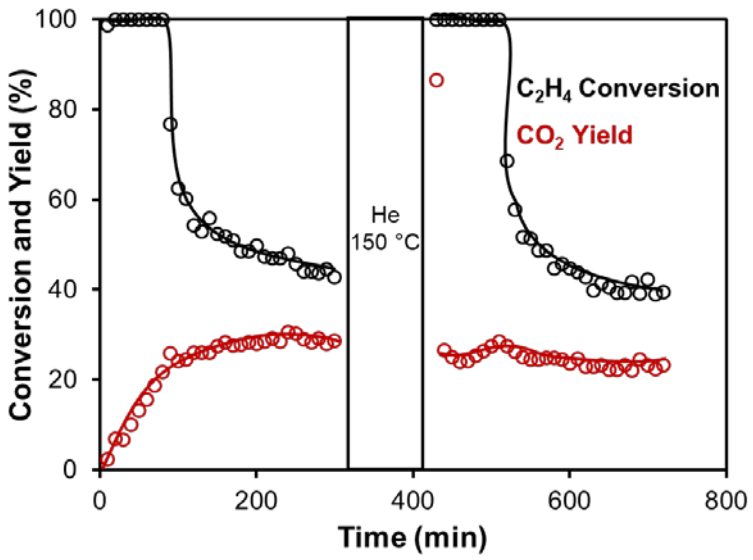


Figure 1. Time courses for aerobic oxidation of trace ethylene over Pt/SBA-15(800) at 0 °C (ethylene oxidation, black circles; CO_2 yield, red circles). Reaction conditions: Pt/SBA-15(800) 0.40 g (1.8 wt% of Pt loading), C_2H_4 50 ppm, N_2 5%, O_2 20%, He balance, SV 1500 mL h^{-1} g^{-1}. After 300 min of the reaction, the catalyst was heated again at 150 °C for 120 min in a He flow (40 mL min^{-1}) and used for subsequent reaction.

We have reported that catalytic activity of SBA-15 supported Pt catalyst depends on hydrophobic nature of the support itself.[18] Calcination of SBA-15 support at 800 °C and subsequent deposition of Pt nanoparticle forms Pt/SBA-15(800), a highly active and durable Pt catalyst in the ethylene oxidation at 0 °C.[18] Figure 1 shows time courses for ethylene conversion and CO_2 yield over Pt/SBA-15(800). Initial activity changed drastically with time in the early stage of the reaction, but both conversion and yield reached constant at approximately 45% and 28%, respectively. The same phenomenon can be observed after heat treatment of the spent Pt/SBA-

15(800) at 150 °C for 120 min in a He flow (40 mL min^{-1}). No significant change between the first and the reuse experiments assures high durability of the catalyst in this reaction. Decrease in initial activity is mainly attributable to intermediates and water that block active Pt sites on fresh catalyst. The difference between conversion and yield will disappear when prolonging the reaction time, which means the reaction reaches actual steady-state.[17] However, extremely low ethylene concentration requires a high SV and a long reaction time to assess the steady-state activity. Referring to our previous paper, there was no apparent change in CO_2 yield in between pre-steady-state at 180-300 min and in actual steady-state, although ethylene conversion gradually decreased with time and became finally equal to CO_2 yield.[17] For the sake of simplicity, therefore, the pre-steady-state activity of all catalysts at 300 min was used for comparison in this study.

Here, Pt/SBA-15(800) was further studied in fair comparison with other Pt catalysts using a nonporous silica support (Aerosil 380 (A380)). Supported Pt catalysts were synthesized with nonporous amorphous silica for reference materials and then subjected to the reaction under the same conditions to clarify the effect of mesoporosity and hydrophobicity. A380 was calcined at 700, 800 and 900 °C before the impregnation of Pt nanoparticles. Table S1 shows structural parameters of parent and calcined A380 after impregnation of Pt nanoparticle. All samples have a type-II isotherm typically observed for nonporous solid materials (Figure S1(B)). Surface area decreased by calcination treatment, but Pt/A380(900) still has high surface area of 240 m^2 g^{-1}. Mesopore volume of these materials (0.39-0.26 mL g^{-1}) is derived from interparticle voids among SiO_2 nanoparticles. The formation of Pt nanoparticle can be confirmed by broad and weak diffractions of metallic Pt in XRD patterns (Figure S1(A)). The average sizes of the Pt particles were estimated by CO adsorption measurements[30–32] to be 4.0-5.0 nm in diameter. TEM analysis also provides a similar value; average size of Pt nanoparticle for Pt/SBA-15 and Pt/SBA-15(800)

was estimated as 6.5 nm and 7.5 nm, respectively, in the previous papers.[17,18] TEM measurement of Pt/A380(800) in this study shows that Pt nanoparticles in size of 5.5 nm are highly dispersed on A380(800) surface (Figures S1(C) and (D)).

Table 1. Structural parameters and catalytic activity for silica-supported Pt catalysts.[a]

	S_{BET}[b] / $m^2\ g^{-1}$	V_{meso}[c] / mL g^{-1}	D_{meso}[d] / nm	CO/Pt[e]	D_{Pt}[f] / nm	Catalytic Activity[i]	
						Conv.[j] (%)	Yield[k] (%)
Pt/SBA-15[18]	867	1.04	12.7	0.16	6.9 (6.5)[g,h]	30	16
Pt/SBA-15(800)[18]	572	0.76	10.1	0.12	9.2 (7.5)[g,h]	45	28
Pt/A380	392	0.39	−	0.25	4.3	30	11
Pt/A380(700)	325	0.32	−	0.30	4.8	35	16
Pt/A380(800)	313	0.32	−	0.23	4.9 (5.5)[g]	35	17
Pt/A380(900)	240	0.26	−	0.23	4.8	37	18

[a]Reaction conditions: catalyst 0.40 g (1.8 wt% of Pt loading), C_2H_4 50 ppm, N_2 5%, O_2 20%, He balance, SV 1500 mL $h^{-1}\ g^{-1}$, temp. 0 °C, time 300 min. [b]BET surface area. [c]Pore volume estimated using the Barrett−Joyner−Halenda (BJH) equation. [d]Average pore diameter estimated by NLDFT. [e]CO/Pt ratio estimated from CO-pulse titration. [f]Average diameter of Pt nanoparticles estimated by CO-pulse titration. [g]Average diameter of Pt nanoparticles inside the mesopores of SBA-15 and SBA-15(800) and over A380(800) using TEM. [h]References 17 and 18. [i]Time 300 min. [j]Ethylene conversion. [k]CO_2 yield.

All reference catalysts using bare and calcined SBA-15 and A380 were also examined in ethylene oxidation for comparison. They showed similar time courses of ethylene oxidation to that of Pt/SBA-15(800) as shown in Figures S2 and S3.[18] Ethylene conversion and CO_2 yield became constant apparently in all cases at 300 min. Table 1 summarizes structural parameters and catalytic

activities of all catalysts examined. There was no significant difference in both conversion and yield at 300 min among all reference catalysts, and these activities were inferior to that of Pt/SBA-15(800). The relatively large size of Pt nanoparticle determined by CO-pulse titration (9.2 nm) and TEM (7.5 nm) reveals that the number of Pt sites on Pt/SBA-15(800) is lower than that of other reference catalysts. Oxidation state of Pt nanoparticle was evaluated by XPS measurement. Figure S4 shows Pt 4f XPS spectra for Pt/SBA-15(800) and Pt/A380(800) before and after the reaction. Fresh Pt/SBA-15(800) and Pt/A380(800) have two symmetric bands at 71.6 and 74.7 eV that are assignable to Pt($4f_{7/2}$) and Pt($4f_{5/2}$) of metallic Pt, respectively.[33] No apparent change in their shape and position was observed for the spent Pt/SBA-15(800) and Pt/A380(800), which reveals that metallic state of Pt nanoparticle is preserved intact after the reaction.

Ethylene oxidation over supported Pt catalysts is not a structure-sensitive reaction, because the activity of Pt/SBA-15 (6.9 nm) was comparable to that of Pt/A380 (4.3 nm). Size effect of Pt nanoparticle is of less importance, because the activity for 1.8 wt% Pt/SBA-15 with 6.2 nm of Pt nanoparticle is almost identical to that for 1.0 wt% Pt/SBA-15 with 5.0 nm of Pt nanoparticle after normalization of ethylene conversion by Pt loading: 1.0wt%Pt/SBA-15 for 1.72 μmol g^{-1}-Pt and 1.8wt% Pt/SBA-15 for 1.83 μmol g^{-1}-Pt at 300 min (Table S2). Therefore, hydrophobicity of silica surface and mesoporosity seems to be controlling factors for high activity of Pt/SBA-15(800) catalyst. We studied hydrophobicity of Pt/SBA-15(800) and three reference catalysts (Pt/SBA-15, Pt/A380, and Pt/A380(800)) using H_2O adsorption and ^{29}Si MAS NMR measurements.

Hydrophobicity of Pt/SBA-15(800) and Reference Catalysts

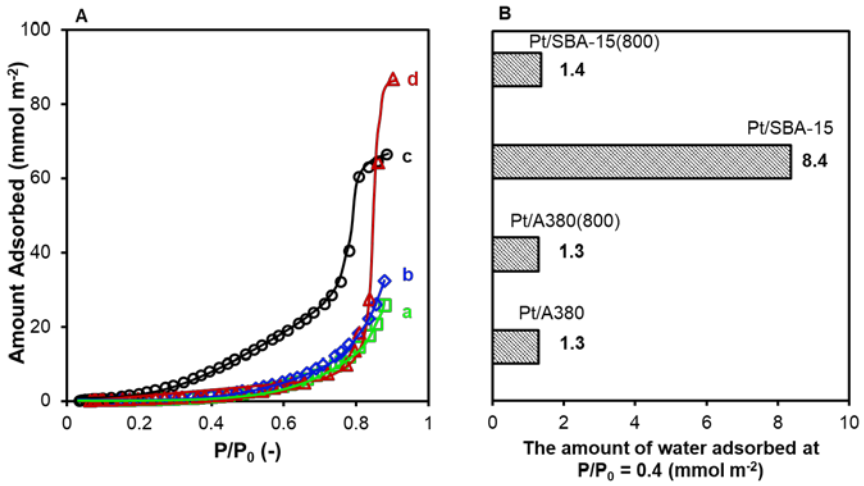


Figure 2. Water adsorption isotherms (A) and the amounts of physisorbed water on Pt/A380 and Pt/SBA-15 estimated from P/P_0=0.4 of their H_2O adsorption isotherms (B). All values in (A) and (B) are normalized with their surface areas. (a), (b), (c), and (d) in (A) are Pt/A380, (b) Pt/A380(800), (c) Pt/SBA-15, and (d) Pt/SBA-15(800), respectively.

Figure 2 shows H_2O adsorption isotherm of these four catalysts at 25 °C, together with the amount of H_2O adsorbed at P/P_0=0.40 per surface area (mmol-H_2O m^{-2}). There is no difference between two A380 catalysts that exhibit a typical type-III isotherm[34] and a similar value of water adsorbed (1.3 mmol-H_2O m^{-2}), which suggests that A380 has highly condensed siloxane network and no influence by a simple calcination treatment at 700−900 °C. While two SBA-15 catalysts also show a typical type-III isotherm as well, the value of water adsorbed was clearly decreased by calcination treatment. Thermal treatment of as-synthesized precursor at 560 °C removes most of surfactant molecules inside mesopores and affords weakly condensed mesoporous SBA-15 with hydrophilic surface that adsorbs a large amount of H_2O (8.4 mmol m^{-2}). Further calcination at high temperature produces hydrophobic surface with a small amount of water adsorbed (1.4 mmol m^{-}

^{2}). No significant difference in catalytic activity of Pt/A380, Pt/A380(800), and other two A380 catalysts in Table 1 is due to similar hydrophilic-hydrophobic property before and after calcination treatment. On the other hand, calcination at 800 °C makes SBA-15 hydrophobic, which improves the activity (Pt/SBA-15(800)).[18] It should be noted that the order of these activities (Pt/SBA-15(800) >> Pt/SBA-15 = Pt/A380(800) = Pt/A380) cannot be simply explained with hydrophobic nature of silica supports (Pt/SBA-15(800) = Pt/A380(800) = Pt/A380 >> Pt/SBA-15).

Water affinity of silica is also related to condensation of silica network, which is quantitatively evaluated with ^{29}Si MAS NMR measurement. Water molecules are preferably adsorbed on polar and hydrophilic SiOH groups through hydrogen-bonding interaction. Condensed silica species that affects hydrophobicity of silica surface can be expressed with Q_4 content to the sum of all Q sites (Q_2+ Q_3+ Q_4), in which $Si(OH)_2(OSi)_2$, $Si(OH)(OSi)_3$, and $Si(OSi)_4$ are denoted as Q_2, Q_3, and Q_4, respectively.[35] Table 2 lists catalytic activities and Q contents (Q_2, Q_3, and Q_4) for four samples. Q sites of the samples can be identified from ^{29}Si MAS NMR spectra by a curve fitting technique (Figures S5 and S6). Q_4 content of SBA-15 and A380 increased with the decrease in Q_2 and Q_3 due to thermal condensation at 800 °C, which gave 84.9% in Pt/SBA-15(800) and 73.5% in Pt/A380(800). Pt/SBA-15(800) consists of highly condensed siloxane network compared to others, but hydrophobicity of Pt/SBA-15(800) itself is apparently comparable to that of Pt/A380(800), due to no difference in the amount of water adsorbed (1.3-1.4 mmol m^{-2}). In addition, the trend in the activity of the catalysts examined is not consistent with the order of Q_4 content (Pt/SBA-15(800) > Pt/SBA-15 = Pt/A380(800) > Pt/A380). These results suggest that Q_4 content is not a crucial parameter to discuss the hydrophobicity of mesoporous silica and nonporous silica. This is probably due to capillary condensation nature of mesoporous materials; mesopores preferably accumulates water molecules by capillary condensation more effectively compared to nonporous

silica. ^{29}Si MAS NMR measurement was also conducted for spent Pt/SBA-15(800) before and after regeneration treatment (Table 2). No difference in Q_2, Q_3, and Q_4 contents between two samples means that original hydrophobicity of Pt/SBA-15(800) kept intact during the reaction and after reactivation treatment.

Table 2. Surface area, Q content, and catalytic activity of Pt/SBA-15(800) and reference catalysts.

	S_{BET}[a] / m^2 g^{-1}	Q Content[b] (%)			Catalytic Activity[c] (%)	
		Q_2	Q_3	Q_4	Conv.[d]	Yield[e]
Pt/SBA-15	867	3.2	22.2	74.7	30	16
Pt/SBA-15(800)	572	0.0	15.1	84.9	45	28
Pt/A380	392	7.7	28.5	63.8	30	11
Pt/A380(800)	313	0.0	26.5	73.5	35	17
Pt/SBA-15(800)-Spent	-	0.0	14.8	85.2	-	-
Pt/SBA-15(800)-Reactivated	-	0.0	14.9	85.1	-	-

[a]BET surface area. [b]Q content (Q_2, $Si(OH)_2(OSi)_2$; Q_3, $Si(OH)(OSi)_3$; Q_4, $Si(OSi)_4$). [c]Reaction conditions: catalyst 0.40 g (Pt 1.8 wt%), C_2H_4 50 ppm, N_2 5%, O_2 20%, He balance, SV 1500 mL h^{-1} g^{-1}, temp. 0 °C. [c]Time 300 min. [d]Ethylene conversion, [e]CO_2 yield.

Water adsorption experiments and ^{29}Si MAS NMR measurements imply that another effect in addition to hydrophobicity contributes to the high activity of Pt/SBA-15(800), because both Pt/SBA-15(800) and Pt/A380(800) have similar affinity toward water. Next, we directly monitored negative impact of physisorbed water on the activity of Pt/SBA-15(800) and reference catalysts using *in-situ* FTIR setup.

Effect of H_2O Vapor on Ethylene Oxidation

Ethylene oxidation was carried out over Pt/SBA-15(800) and three reference catalysts with/without water vapor (approximately 0.95 vol%). The reactions were conducted in an IR cell connected to a gas flow system, where inlet and outlet gases were analyzed with GC to determine ethylene conversion and CO_2 yield. Change in the amount of physisorbed water on catalyst surface was simultaneously monitored with FTIR. Figure 3 shows time courses for ethylene oxidation over supported Pt catalysts, together with time dependence on normalized band intensities of OH bending mode of physisorbed water on the basis of sample weight. A high temperature (28°C) with a relatively large SV of 15,000 mL h^{-1} g^{-1} was adopted in these reactions to maintain ethylene conversion at 40−60% before introduction of water vapor. Continuous decrease in both conversion and CO_2 yield was observed in all catalysts in initial 3 h, which indicates these reactions do not reach steady state. It was clear that the activity of Pt/SBA-15(800) at 3 h is higher than those of other catalysts under the reaction conditions. After the supply of water vapor from 3 h, the activity (conversion and yield) of all catalysts decreased more steeply with time and reached less than 10% at around 6 h. In contrast, band intensities of physisorbed water in all reactions increased drastically and reached almost maximum by 5 h. These results indicate that the amount of physisorbed water on catalyst surface is an important factor governing the activity of supported Pt catalyst. When water-supply was stopped and the reactions continued in the dry conditions, the activity of all catalysts was gradually recovered with time. The recovery of the activity was correlated with the decrease in the amount of physisorbed water and the activity of Pt/SBA-15(800) was quickly recovered compared to others. For further quantitative discussion, normalized band intensities and catalytic activities obtained from Figure 3 were compared in Table 3.

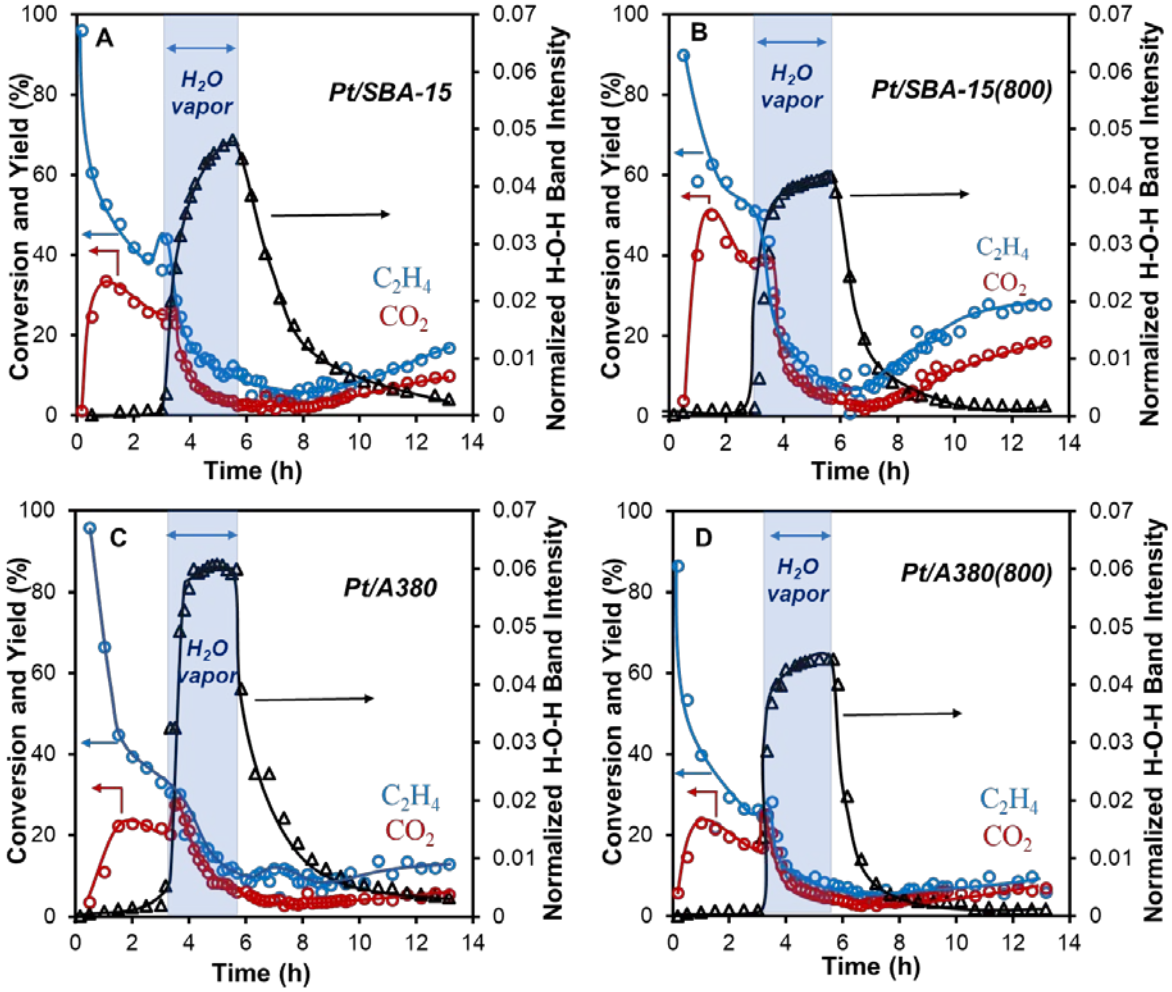


Figure 3. Time courses for ethylene oxidation and normalized bending vibration of physisorbed H_2O over Pt/SBA-15 (A), Pt/SBA-15(800) (B), Pt/A380 (C) and Pt/A380(800) (D). Reaction conditions: catalyst 0.04 g (Pt 1.8 wt%), C_2H_4 50 ppm, O_2 20%, N_2 5%, He balance, SV 15000 mL h^{-1} g^{-1}, temp. 28 °C, water content 0.95%.

Table 3. Comparison of band intensity of physisorbed H_2O and activity of the catalysts.

	Normalized band intensity of H_2O bending mode in Figure 3		Catalytic activity at 10 h in Figure 3	
	5 h	10 h	Conversion (%)	Yield (%)
Pt/SBA-15	0.048	0.0067	11.7	6.1
Pt/SBA-15(800)	0.041	0.0013	21.1	12.6
Pt/A380	0.060	0.0053	9.7	4.5
Pt/A380(800)	0.044	0.0013	7.4	6.1

The samples have an intense OH bending vibration band with normalized intensity of 0.04-0.06 after complete hydration of catalyst surfaces at 5 h. The band intensity of two calcined samples (Pt/SBA-15(800) and (Pt/A380(800)) decreased more drastically than that of non-calcined Pt/SBA-15 and Pt/A380 and became negligibly small (ca. 0.0013) at 10 h. Note that the activity of Pt/SBA-15(800) is twice that of Pt/A380(800), despite no significant difference in hydration state between two samples; ethylene conversion and CO_2 yield of Pt/SBA-15(800) and Pt/A380(800) are 21.1% and 12.6%, and 7.4% and 6.1%, respectively.

The high activity cannot be still rationalized by the water content of silica surface based on normalized band intensity, as observed with Pt/SBA-15(800) and Pt/A380(800). It should be noted that the size of Pt nanoparticle on Pt/SBA-15(800) (7.5 nm) is larger than that on Pt/A380(800) (5.5 nm). This difference suggests that Pt/A380(800) has a large number of active Pt sites for ethylene oxidation in comparison to Pt/SBA-15(800) if both samples are hydrated to the similar extent. In order to investigate the difference in Pt sites of Pt/SBA-15(800) and Pt/A380(800) in the presence or absence of physisorbed water, *in-situ* FTIR measurements were carried out using CO as a probe molecule.

In-situ FTIR Measurements for Pt/SBA-15(800) and Pt/A380(800)

Pt/SBA-15(800) in the pellet form was heated in the IR cell at 150 °C for 2 h and the dried sample was exposed to a He stream (10 mL min^{-1}) containing 0.95% of water vapor for 160 min to saturate its surface with physisorbed water. CO adsorption experiment was then conducted with the hydrated Pt/SBA-15(800) where CO with 100 ppm was added to the gas stream of He/H_2O mixture. Figure 4(A) shows difference FTIR spectra of hydrated Pt/SBA-15(800) before and after CO adsorption. The IR spectrum of dried Pt/SBA-15(800) was used as background throughout the experiments. Introduction of He/H_2O gas mixture to Pt/SBA-15(800) forms two positive bands at 3600-3000 cm^{-1} and 1628 cm^{-1} for stretching and bending vibration modes of physisorbed water, and their intensities reach constant after 60 min. A broad feature of OH stretching vibration, together with a negative band at 3735 cm^{-1} attributable to OH stretching mode of SiOH group, indicates that hydrogen bonding network among physisorbed water molecules and SiOH groups is highly developed on the surface. When CO was introduced with He/H_2O to fully hydrated surface of Pt/SBA-15(800), a new band for Pt–CO appeared in 2100-2000 cm^{-1} region without significant change in the intensity for OH stretching and bending vibration bands. The formation of Pt–CO band suggests the presence of free Pt sites available or exchange between physisorbed water on Pt surface and CO took place. Time dependence on the vibration band for the Pt–CO species was highlighted in Figure 4(B). Two distinct bands were observed at 2090 cm^{-1} and 2075 cm^{-1} and increased their intensity with time, reaching constant after 150 min. The former band can be observed after the introduction of a dry CO/He gas to dehydrated Pt/SBA-15(800) as shown in Figure 4(C); the latter band is therefore most likely due to the interaction of Pt–CO species with physisorbed water through hydrogen-bonding force, which induces the red-shift of original Pt–CO band observed for dehydrated Pt/SBA-15(800).

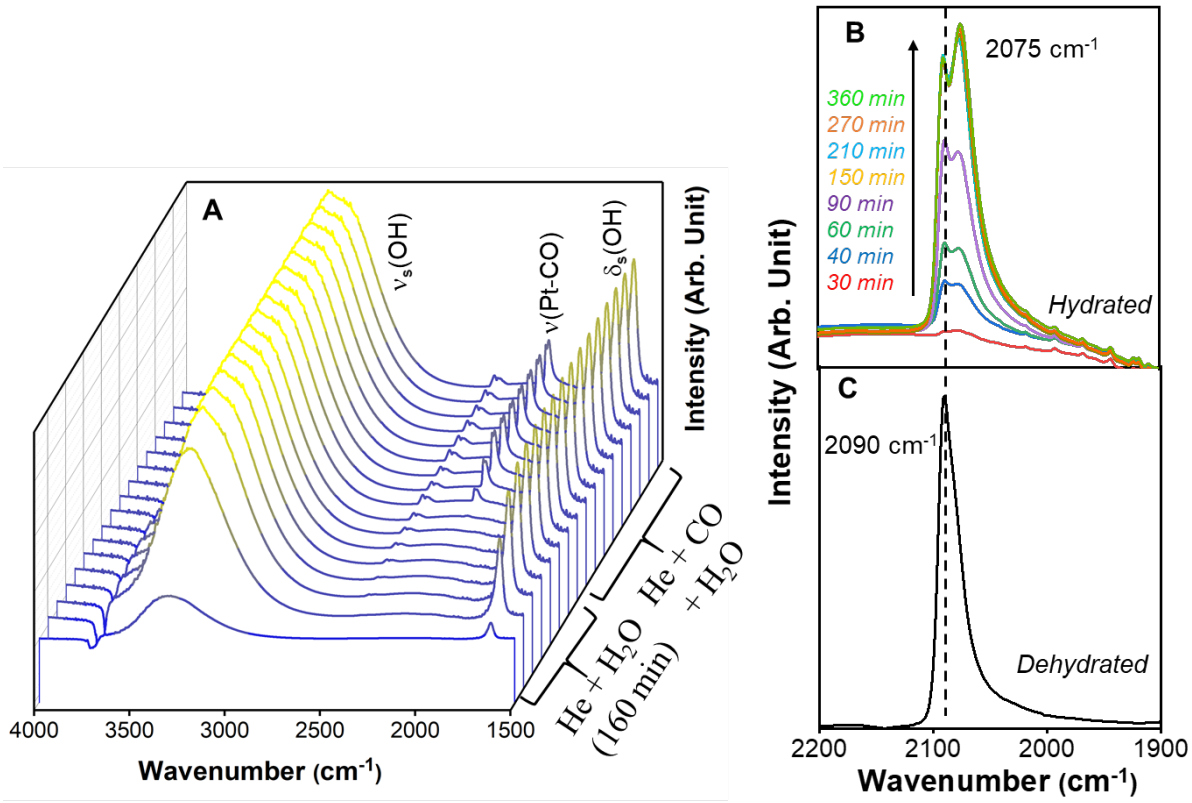


Figure 4. Difference FTIR spectra of Pt/SBA-15(800) under the flow of He/H_2O mixture for 160 min and the flow of He/CO/H_2O for additional 360 min (A). Change in Pt–CO band in difference FTIR spectra of hydrated Pt/SBA-15(800) in (A) under the flow of He/CO/H_2O for 360 min (B). Difference FTIR spectrum of CO–adsorbed dehydrated Pt/SBA-15(800) (C).

Distinct results were obtained from a series of same experiments using Pt/A380(800) (Figure 5): dehydrated Pt/A380(800) was fully hydrated with water vapor by the treatment of H_2O/He gas, and hydrated Pt/A380(800) offered Pt sites for the formation of Pt–CO species under a H_2O/CO/He flow (Figure 5(A)). Figure 5(B) shows time dependence on the Pt–CO band in difference FTIR spectra of hydrated Pt/A380(800) under a H_2O/CO/He flow. The formation of Pt–CO species afforded a single band at 2073 cm^{-1} and its intensity increased with time, reaching almost constant

after 150 min. Pt–CO species on dehydrated Pt/A380(800) forms a single band at 2083 cm^{-1}, which is different from that on hydrated Pt/A380(800). This red-shift is also due to the interaction of Pt–CO species with water molecule.

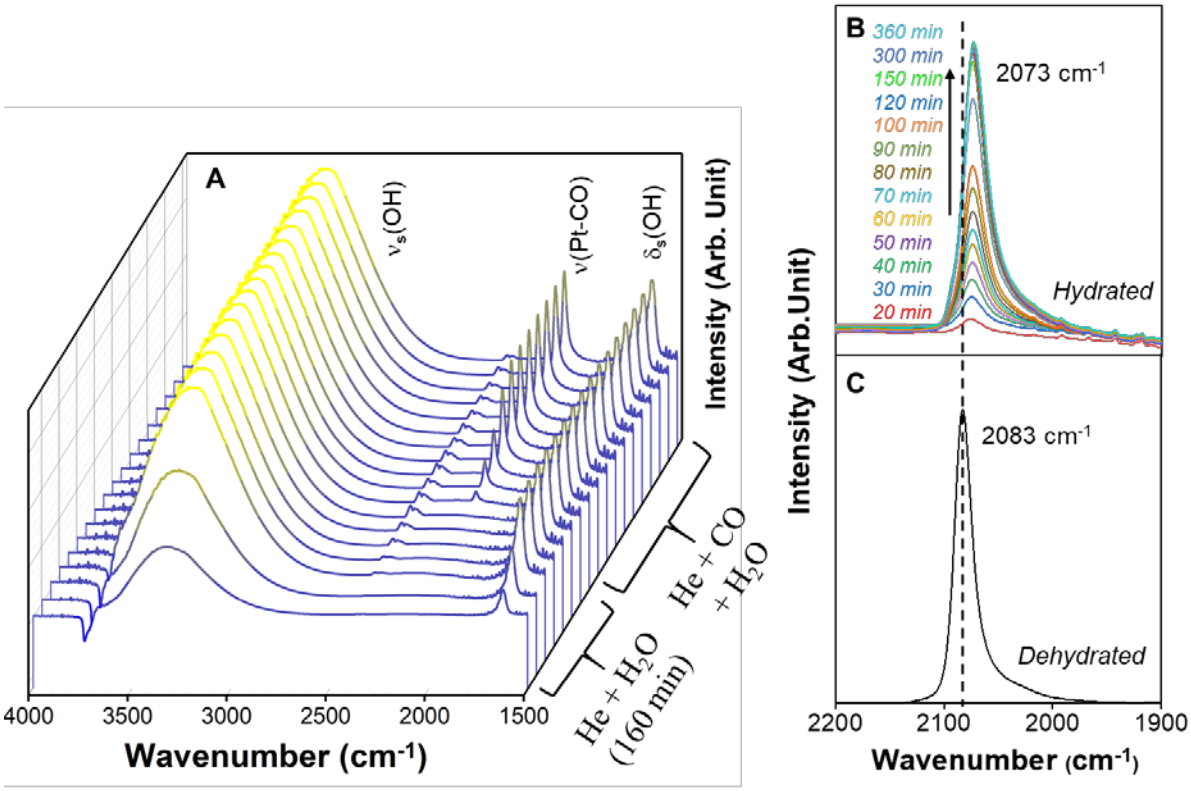
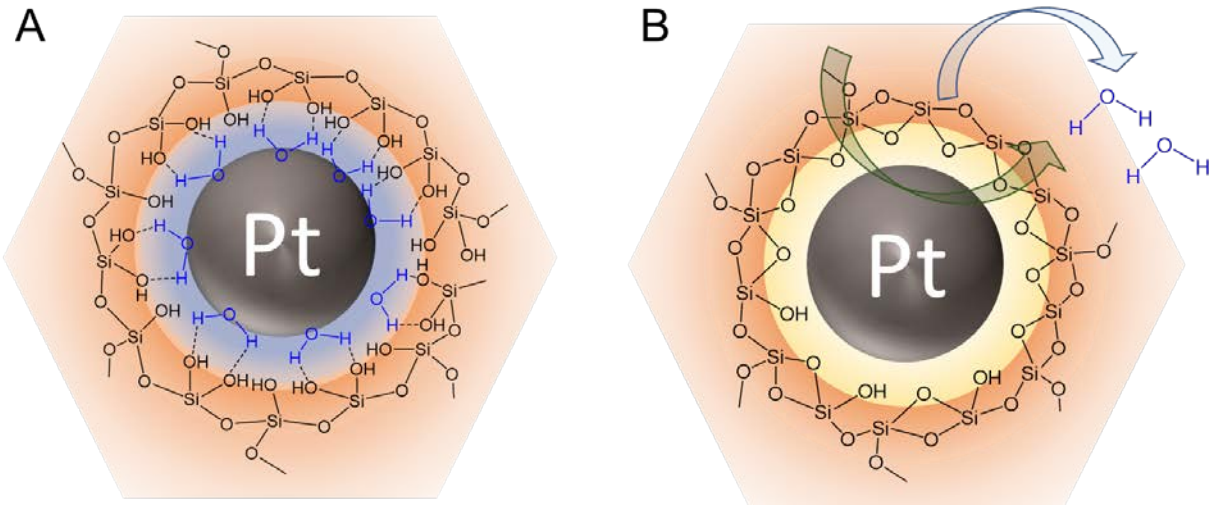


Figure 5. Difference FTIR spectra of Pt/A380(800) under the flow of He/H_2O mixture for 160 min and the flow of He/CO/H_2O for additional 360 min (A). Change in Pt–CO band in difference FTIR spectra of hydrated Pt/A380(800) in (A) under the flow of He/CO/H_2O for 360 min (B). Difference FTIR spectrum of CO–adsorbed dehydrated Pt/A380(800) (C).

The difference between Pt/SBA-15(800) and Pt/A380(800) is attributed simply to anhydrous Pt sites present on fully hydrated surface of Pt/SBA-15(800). Dehydrated Pt/SBA-15(800) and Pt/A380(800) have the band assignable to linear Pt–CO vibration at 2090 and 2083 cm^{-1}.[36–38] This deviation may be derived from the difference in the density of silanol group (Table 2 and Figure S5). Silanol group have weak acidity (positively charged proton) that affects electronic state of Pt nanoparticle. A380(800) is more prominent for this effect due to high content of Q_3 site. Saturation of catalyst surface with physisorbed water forms rigid hydrogen-bonding network among water molecules and silanol groups in both samples as evidenced by the new bands for OH stretching and bending modes (Figures 4(A) and 5(A)). Introduction of CO to hydrated surface of Pt/SBA-15(800) and Pt/A380(800) results in the formation of Pt–CO bond in the hydrogen-bonding network, which shifts its band position to low wavenumber region: Pt–CO band on hydrated Pt/SBA-15(800) and Pt/A380(800) appears at 2075 and 2073 cm^{-1}, respectively. A single Pt–CO band present in hydrated Pt/A380(800) strongly suggests that Pt and SiO_2 surfaces of Pt/A380(800) are covered with hydrogen-bonding network entirely and all CO molecules on Pt surface are inevitably involved in the hydrogen-bonding network. On the other hand, hydrated Pt/SBA-15(800) has an additional Pt–CO band at 2090 cm^{-1}, which is identical to Pt–CO band formed on dehydrated Pt/SBA-15(800). The results for dehydrated and hydrated Pt/SBA-15(800) imply the presence of bare Pt sites on Pt/SBA-15(800) even after the saturation of its surface with water vapor.

This unique feature can be likely linked with high activity of Pt/SBA-15(800). As shown in Figures 1 and 3, the activity of supported Pt catalyst decreased with time, due to the presence of physisorbed water molecules. The change in the activity is most probably due to the decrease in the number of active Pt sites for ethylene oxidation by direct physisorption of water on Pt surface.

The formation of hydrogen-bonding network around Pt nanoparticle will prevent access of reactant molecules including ethylene and oxygen, which is also another possible factor to affect the activity. Bare Pt sites without interaction of physisorbed water through hydrogen-bonding force can be formed on fully hydrated Pt/SBA-15(800) and work as catalytically active sites in ethylene oxidation more effectively than hydrated Pt sites present in hydrogen-bonding network. We attribute the formation of such unique Pt sites to both “mesoporosity” and “hydrophobic silica surface” of SBA-15(800) support in terms of less activity of three reference catalysts (Pt/SBA-15, Pt/A380, and Pt/A380(800).



Scheme 1. Schematic representation of a Pt nanoparticle inside a hydrophilic mesopore (A) and a hydrophobic mesopores (B) of SBA-15(800).

Presumable structure of hydrophobic Pt sites is proposed in Scheme 1. Due to highly developed porous structure, most of Pt nanoparticles on SBA-15-supported Pt catalysts are stabilized inside mesopores and surrounded with siloxane network. A close distance between siloxane moiety on internal mesopore wall and surface Pt sites of Pt nanoparticles enables efficient removal of water molecules formed on silica surface through the formation of hydrogen-bonding network, which

makes the Pt sites active in ethylene oxidation. However, hydrogen-bonding network is getting developed among physisorbed water molecules and silanol groups with time, and all Pt sites available for ethylene oxidation are finally included in the hydrogen-bonding network at the steady-state. Pt sites on hydrated surface are able to promote ethylene oxidation, but they are less active than those on dehydrated surface, which reflects the difference in the activity between at the initial stage and at steady state.

In contrast, calcination treatment of SBA-15 at 800 °C decreases the density of SiOH groups and then produces hydrophobic SiO_2 surface inside mesopores. Distribution of SiOH group is not homogeneous and SBA-15(800) has both hydrophobic and hydrophilic mesopores. Pt nanoparticles inside hydrophilic mesopores are finally involved in hydrogen-bonding network formed and exhibit similar activity to those of hydrophilic Pt/SBA-15. These Pt sites in hydrogen-bonding network can be expressed by Pt–CO band at 2075 cm^{-1} in Figure 4. Pt nanoparticles inside hydrophobic mesopores are, however, always free from hydrogen-bonding network even after saturation of the catalyst surface with physisorbed water, as evidenced by Pt–CO band at 2090 cm^{-1} in Figure 4. These "Pt nanoparticles inside hydrophobic mesopores" make Pt/SBA-15(800) active in the presence of water compared to other reference catalysts. Hydrophobic mesopores will facilitate desorption of water molecules from Pt surface and subsequently remove them from the mesopores. This feature will enable quick recovery of the activity as observed in Figure 3(B). Pt/SBA-15(800) is distinct from Pt/A380(800) in terms of "mesoporous structure". In the case of A380, Pt nanoparticles are simply immobilized with flat SiO_2 surface and total Pt surface area interacted with SiO_2 is extremely small compared to that of Pt/SBA-15(800). Therefore, all Pt sites on Pt/A380(800) work moderately in the hydrogen-bonding network.

We further observed the interaction between Pt–CO and H_2O molecule on Pt/SBA-15(800) and Pt/A380(800) using FTIR. These two samples were heated at 150 °C for 2 h to remove physisorbed water and then saturated with CO under a stream of CO/He gas (100 ppm of CO, 10 mL min^{-1}). CO-saturated samples were exposed to a stream of water vapor (H_2O/He, 0.95 vol.%) and the change in the band of Pt–CO vibration mode as well as the band of H_2O bending mode was monitored from time dependence of difference FTIR spectra.

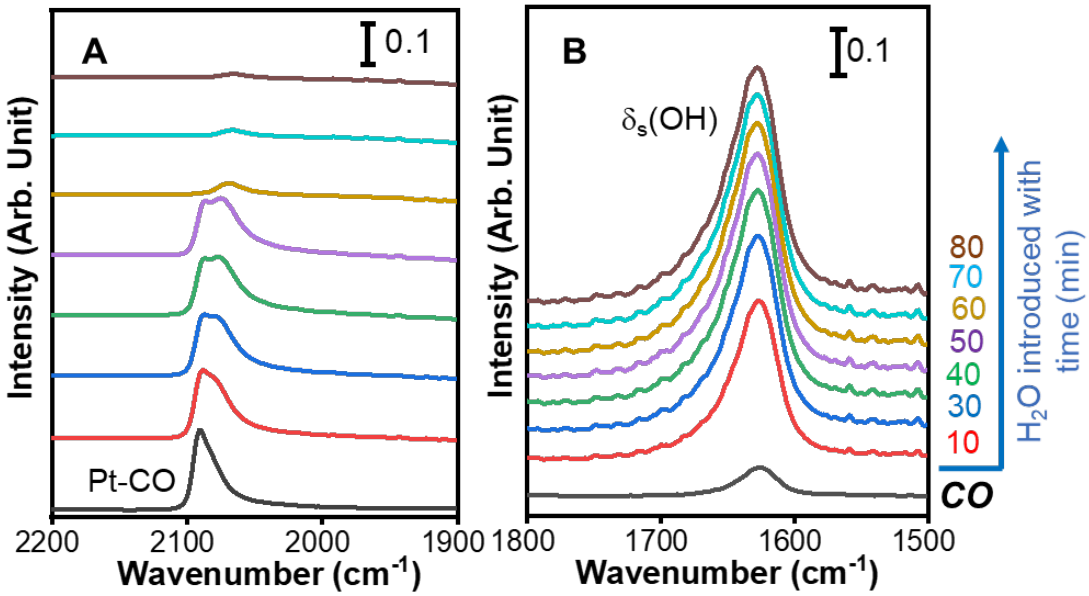


Figure 6. Difference FTIR spectra of CO-adsorbed Pt/SBA-15(800) in a stream of H_2O-He gas mixture. (A) and (B) shows Pt–CO band and H_2O bending mode regions of the spectra, respectively.

Figure 6 shows difference FTIR spectra of CO-saturated Pt/SBA-15(800) taken during the treatment with a water vapor stream, in which A and B correspond to Pt–CO vibration (2200-1900

cm^{-1}) and H_2O bending vibration (1800-1500 cm^{-1}) regions. The band intensity of H_2O bending mode monotonically increased with time and reached maximum at 60 min, suggesting that Pt/SBA-15(800) is quickly hydrated with physisorbed water. Drastic change was detected in Pt–CO band region. The original Pt–CO band on 2090 cm^{-1} is present on fresh samples. A new shoulder band at 2075 cm^{-1} appears after 10 min of H_2O vapor treatment and its intensity increases with time and reaches maximum at 50 min, whereas original Pt–CO band at 2090 cm^{-1} remains with slight decrease in its intensity. According to previous discussion, the Pt–CO band at 2075 cm^{-1} is attributed to hydrogen-bonding interaction of CO on Pt surface with H_2O molecule, which suggests that certain amount of CO molecules adsorbed on Pt nanoparticles inside hydrophilic mesopores participates in the formation of hydrogen-bonding network and then gives a new band at 2075 cm^{-1}. The presence of original Pt–CO band means that CO molecules on Pt nanoparticles inside hydrophobic mesopores are isolated from hydrogen-bonding interaction. These two bands become weak at 60 min and negligibly small after 70 min, due to desorption of CO under the gas stream. Additional experiments were conducted after 80 min. The fully hydrated sample was again exposed to a dry CO/He mixture with CO concentration of 100 ppm and change of difference FTIR spectra was monitored with time as shown in Figure S7. The band intensity of H_2O bending mode decreased with time due to desorption of physisorbed water under dry conditions. Pt–CO band at 2090 cm^{-1} appeared from 30 min. Two bands for linear Pt–CO species at 2090 and 2075 cm^{-1} increased their intensity from 30 min and became prominent at 100 min due to desorption of physisorbed water molecules. The reason to observe these two bands simultaneously is attributable to incomplete desorption of physisorbed water that keeps the band at 2075 cm^{-1} even at 100 min. This reversible change in two bands under wet or dry conditions is a direct evidence for no

reconstruction of Pt surface by adsorbed CO[22,39,40] but physisorbed water affecting band position of linear Pt–CO band on Pt/SBA-15.

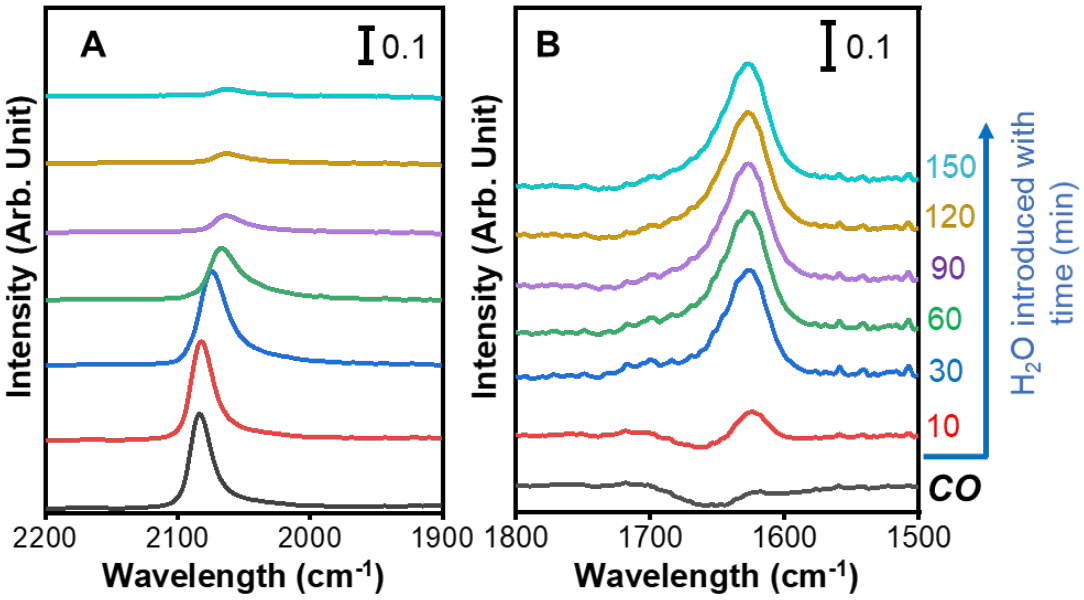


Figure 7. FTIR spectra showing bands of Pt–CO and v(HOH) interaction during CO replacement by H_2O molecules over Pt/A380(800) (A), (B).

Same experiment was conducted with Pt/A380(800). Figure 7 shows difference FTIR spectra of CO-saturated Pt/A380(800) taken during the treatment with a water vapor stream. It should be noted that Pt–CO band always appears as a single band throughout the experiment. Original band at 2083 cm^{-1} was gradually red-shifted with the increase in physisorbed water (evidenced by the increase in band intensity of H_2O bending vibration) and was finally present at 2064 cm^{-1}. Desorption of CO molecules after 60 min results in the decrease in band intensity and most of CO molecules on Pt surface disappears after 90 min. These changes are clearly distinct from those of Pt/SBA-15(800). This continuous change happened reversibly under a dry CO/He flow as observed for Pt/SBA-15(800). A dry CO/He gas (CO concentration, 100 ppm) was introduced to

the hydrated sample after 150 min in which weak Pt–CO band appeared at 2064 cm^{-1}. The Pt–CO band changed its intensity and position continuously with time and finally appears as an intense band at 2083 cm^{-1} (Figure S8), which is almost identical to the original Pt–CO band of dehydrated Pt/A380 (Figure 5(C)). This continuous and reversible shift of a single Pt–CO band on Pt/A380 also excludes surface reconstruction of Pt nanoparticle by adsorbed CO.[22,39,40] Finally, interaction of Pt–CO species with physisorbed water through hydrogen-bonding interaction was studied with density functional theory (DFT) calculations in order to support our interpretations by CO adsorption experiments using FTIR.

DFT Calculations for the Interaction of Pt–CO Species with Physisorbed H_2O

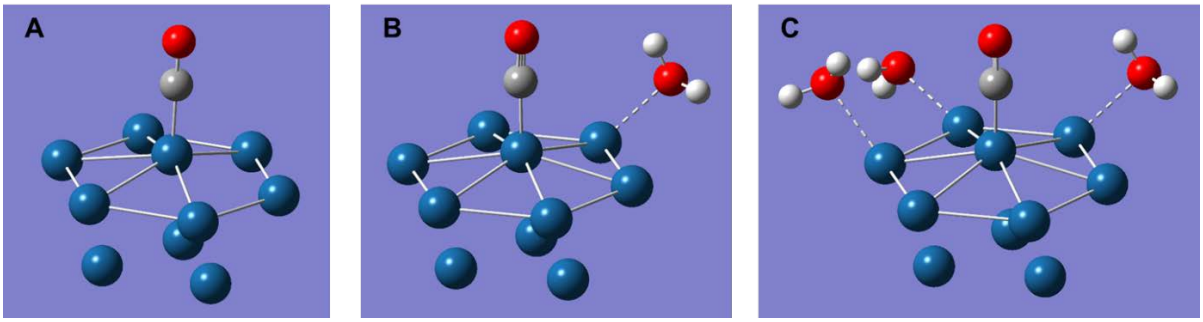


Figure 8. Optimized structures of $Pt_{10}CO$ (A), $Pt_{10}CO(H_2O)$ (B) and $Pt_{10}CO(H_2O)_3$ (C) obtained by the DFT calculations at the B3LYP/LanL2DZ (Pt)/6-31G(d,p) (C,H,O). Indigo: Pt; gray: C; red: O; white: H.

A Pt_{10} cluster model was employed to simulate the adsorption of CO on Pt(111) surface (see Experimental). First, the stretching vibration mode of water-free CO species on Pt (Figure 8(A)) is calculated to be 2072 cm^{-1}, which roughly matches the actual vibration frequency (Table 4). The addition of one water molecule on a Pt atom adjacent to the center one (Figure 8(B)) caused red

shift for CO vibration by 16 cm^{-1} to 2056 cm^{-1}. Further addition of two water molecules (Figure 8(C)) shifted the frequency by 34 cm^{-1} to 2038 cm^{-1}. The red shift is consistent with the observation in actual experiments where the addition of water decreased the CO vibration frequency by 15 cm^{-1} (Figure 4).

Table 4. Summary of DFT calculations.

Structure	ν(C–O) /cm^{-1}	Interatomic distance /Å		CM5 charge		
		Pt–C	C–O	Center Pt	CO	H_2O
$Pt_{10}CO$	2072	1.873	1.151	+0.195	–0.054	–
$Pt_{10}CO(H_2O)$	2056	1.871	1.153	+0.190	–0.078	+0.149
$Pt_{10}CO(H_2O)_3$	2038	1.858	1.157	+0.184	–0.112	av. +0.127

The red shift was clarified by detailed analysis of the geometry and electronic structure. The C–O interatomic distance increased from 1.151 Å to 1.153 Å (one water) and 1.157 Å (three water), suggesting decrease in the bond order. The second-order perturbation theory analysis[29] represented that the back-donation from Pt d-orbital to CO π^* orbital increased by 9 kJ mol^{-1} and by 21 kJ mol^{-1} in the presence of one and three water molecules, respectively. These results indicate that the coordination of water to Pt surface increases the back donation and weakens the C≡O bond strength. This is due to the increased d-electron density of Pt atoms by the electron donation from water molecules. Indeed, the CM5 atomic charge analysis has shown that charges of the central Pt and CO gradually shift to negative by the coordination of water molecules, while the water molecules are positively charged. Consequently, water adsorption near the CO adsorption sites causes red shift of CO vibration owing to electron donation. Taking this theoretical evidence into account,

the partial preservation of CO vibration frequency after introduction of moisture on Pt/SBA-15(800), namely the most hydrophobic catalyst, indicates the presence of water-resistant Pt sites.

CONCLUSION

In-situ FTIR characterization of Pt/SBA-15(800) and Pt/A380(800) using CO as a probe molecule allowed us to clarify unique feature of Pt/SBA-15(800) and the role of hydrophobic silica and mesoporous structure. CO adsorption experiments revealed that incorporation of Pt nanoparticles into hydrophobic mesopores of SBA-15(800) produces bare Pt sites in the presence of water vapor and after saturation of catalyst surface with physisorbed water. This phenomenon was only observed for Pt/SBA-15(800) and can therefore be related to high activity in aerobic oxidation of trace ethylene at 0 °C. Mesopore wall consisting of condensed siloxane network affords hydrophobic interior that enhances smooth desorption of water molecules formed during ethylene oxidation and keeps Pt nanoparticles effective after reaching steady-state. Further control of local environment based on silica, mesoporous structure, and Pt nanoparticle will enable the development of more active silica-supported Pt catalyst aiming for storage and transportation of agricultural products.

ASSOCIATED CONTENT

AUTHOR INFORMATION

Corresponding Author

*Correspondence to Atsushi Fukuoka (fukuoka@cat.hokudai.ac.jp)

Author Contributions

S.S.S., J.H., K.N. and A.F. designed the study. S.S.S. performed all experiments with the assistance of J.H. H.K. conducted the DFT calculations. All authors wrote the paper.

Funding Sources

The authors declare no competing financial interest.

ABBREVIATIONS

FTIR, Fourier-transform infrared spectroscopy; A380, a fumed silica Aerosil 380; SBA-15, a mesoporous silica synthesized with an amphiphilic block copolymer P123; P123, an amphiphilic triblock copolymer consisting of ethylene glycol and propylene glycol moieties; XRD, X-ray diffraction; BET, Brunauer-Emmett-Teller equation; NLDFT, nonlocalized density functional theory; ^{29}Si MAS NMR, ^{29}Si magic angle spinning nuclear magnetic resonance; XPS, X-ray photoelectron spectroscopy; SV, space velocity; GC, gas chromatography; DFT, density functional theory.

Supporting Information: Setup of the fixed-bed flow reactors for ethylene oxidation with supported Pt catalysts, setup of the fixed-bed flow reactor with IR-cell for measurement of *in-situ* FTIR studies, physicochemical properties of Pt/A380 calcined at different temperatures, crystallite size of Pt nanoparticle and catalytic activity for Pt/SBA-15 with different Pt loading, XRD patterns, N_2 adsorption isotherms, and TEM for Pt/A380 samples, time courses for ethylene conversion and CO_2 yield for Pt/A380 and Pt/SBA-15 samples, XPS spectra of Pt/SBA-15(800) and Pt/SBA-15(800) before and after the reaction, ^{29}Si MAS NMR for Pt/SBA-15 and Pt/A380 samples, ^{29}Si MAS NMR for spent and regenerated Pt/SBA-15(800), FTIR spectra of water-adsorbed Pt/SBA-

15(800) in a stream of CO-He, FTIR spectra of water-adsorbed Pt/A380(800) in a stream of CO-He.

REFERENCES

(1) Illeperuma, C. K.; Jayasuriya, P. Prolonged Storage of “Karuthacolomban” Mango by Modified Atmosphere Packaging at Low Temperature. *J. Hortic. Sci. Biotechnol*. **2002**, *77*, 153–157.

(2) Cisneros, L.; Gao, F.; Corma, A. Silver Nanocluster in Zeolites. ADSORPTION of ETHYLENE Traces for Fruit Preservation. *Microporous Mesoporous Mater.* **2019**, *283*, 25–30.

(3) Kou, Y.; Sun, L.-B. Size Regulation of Platinum Nanoparticles by Using Confined Spaces for the Low-Temperature Oxidation of Ethylene. *Inorg. Chem.* **2018**, *57*, 1645–1650.

(4) Ahn, H. G.; Choi, B. M.; Lee, D. J. Complete Oxidation of Ethylene over Supported Gold Nanoparticle Catalysts. *J Nanosci Nanotechnol* **2006**, *6*, 3599–3603.

(5) Isaifan, R. J.; Ntais, S.; Baranova, E. A. Particle Size Effect on Catalytic Activity of Carbon-Supported Pt Nanoparticles for Complete Ethylene Oxidation. *Appl. Catal. A Gen*. **2013**, *464–465*, 87–94.

(6) Li, W.; Zhang, Z.; Wang, J.; Qiao, W.; Long, D.; Ling, L. Low Temperature Catalytic Combustion of Ethylene over Cobalt Oxide Supported Mesoporous Carbon Spheres. *Chem. Eng. J*. **2016**, *293*, 243–251.

(7) Imanaka, N.; Masui, T.; Terada, A.; Imadzu, H. Complete Oxidation of Ethylene at Temperatures below 100 °C over a $Pt/Ce_{0.64}Zr_{0.16}Bi_{0.20}O_{1.90}/\gamma\text{-}Al_2O_3$ *Catalyst. Chem. Lett.* **2008**, *37*, 42–43.

(8) Rojluechai, S.; Chavadej, S.; Schwank, J. W.; Meeyoo, V. Catalytic Activity of Ethylene Oxidation over Au, Ag and Au-Ag Catalysts: Support Effect. *Catal. Commun.* **2007**, *8*, 57–64.

(9) Wicaksana, Y.; Liu, S.; Scott, J.; Amal, R. Tungsten Trioxide as a Visible Light Photocatalyst for Volatile Organic Carbon Removal. *Molecules* **2014**, *19*, 17747–17762.

(10) Li, J.; Ma, C.; Xu, X.; Yu, J.; Hao, Z.; Qiao, S. Efficient Elimination of Trace Ethylene over Nano-Gold Catalyst under Ambient Conditions. *Environ. Sci. Technol.* **2008**, *42*, 8947–8951.

(11) Xue, W. J.; Wang, Y. F.; Li, P.; Liu, Z. T.; Hao, Z. P.; Ma, C. Y. Morphology Effects of Co_3O_4 on the Catalytic Activity of Au/Co_3O_4 Catalysts for Complete Oxidation of Trace Ethylene. *Catal. Commun.* **2011**, *12*, 1265–1268.

(12) Ma, C. Y.; Mu, Z.; Li, J. J.; Jin, Y. G.; Cheng, J.; Lu, G. Q.; Hao, Z. P.; Qiao, S. Z. Mesoporous Co_3O_4 and Au/Co_3O_4 Catalysts for Low-Temperature Oxidation of Trace Ethylene. *J. Am. Chem. Soc.* **2010**, *132*, 2608–2613.

(13) Yang, H.; Ma, C.; Zhang, X.; Li, Y.; Cheng, J.; Hao, Z. Understanding the Active Sites of Ag/Zeolites and Deactivation Mechanism of Ethylene Catalytic Oxidation at Room Temperature. *ACS Catal.* **2018**, 8, 1248–1258.

(14) Yang, H.; Ma, C.; Li, Y.; Wang, J.; Zhang, X.; Wang, G. Synthesis, Characterization and Evaluations of the Ag/ZSM-5 for Ethylene Oxidation at Room Temperature: Investigating the Effect of Water and Deactivation. *Chem. Eng. J.* **2018**, *347*, 808–818.

(15) Yang, H.; Ma, C.; Wang, G.; Sun, Y.; Cheng, J.; Zhang, Z.; Zhang, X.; Hao, Z. Fluorine-Enhanced Pt/ZSM-5 Catalysts for Low Temperature Oxidation of Ethylene. *Catal. Sci. Technol.* **2018**, *8*, 1988–1996.

(16) Jiang, C.; Hara, K.; Fukuoka, A. Low-Temperature Oxidation of Ethylene over Platinum Nanoparticles Supported on Mesoporous Silica. *Angew. Chem., Int. Ed.* **2013**, *52*, 6265–6268.

(17) Satter, S. S.; Yokoya, T.; Hirayama, J.; Nakajima, K.; Fukuoka, A. Oxidation of Trace Ethylene at 0 °c over Platinum Nanoparticles Supported on Silica. *ACS Sustain. Chem. Eng.* **2018**, 6, 11480–11486.

(18) Satter, S. S.; Hirayama, J.; Nakajima, K.; Fukuoka, A. Low Temperature Oxidation of Trace Ethylene over Pt Nanoparticles Supported on Hydrophobic Mesoporous Silica. *Chem. Lett.* **2018**, *47*, 1000–1002.

(19) Hara, K.; Akahane, S.; Wiench, J. W.; Burgin, B. R.; Ishito, N.; Lin, V. S. Y.; Fukuoka, A.; Pruski, M. Selective and Efficient Silylation of Mesoporous Silica: A Quantitative Assessment of Synthetic Strategies by Solid-State NMR. *J. Phys. Chem. C* **2012**, *116*, 7083–7090.

(20) Jaroniec, C. P.; Kruk, M.; Jaroniec, M.; Sayari, A. Tailoring Surface and Structural Properties of MCM-41 Silicas by Bonding Organosilanes. *J. Phys. Chem. B* **1998**, *102*, 5503–5510.

(21) Matsubu, J. C.; Yang, V. N.; Christopher, P. Isolated Metal Active Site Concentration and Stability Control Catalytic CO_2 Reduction Selectivity. *J. Am. Chem. Soc.* **2015**, *137*, 3076–3084.

(22) DeRita, L.; Dai, S.; Lopez-Zepeda, K.; Pham, N.; Graham, G. W.; Pan, X.; Christopher, P. Catalyst Architecture for Stable Single Atom Dispersion Enables Site-Specific Spectroscopic and Reactivity Measurements of CO Adsorbed to Pt Atoms, Oxidized Pt Clusters, and Metallic Pt Clusters on TiO_2. *J. Am. Chem. Soc.* **2017**, *139*, 14150–14165.

(23) Frisch, M. J.; Trucks, G. W.; Schlegel, H. B.; Scuseria, G. E.; Robb, M. A.; Cheeseman, J. R.; Scalmani, G.; Barone, V.; Petersson, G. A.; Nakatsuji, H.; Li, X.; Caricato, M.; Marenich, A. V.; Bloino, J.; Janesko, B. G.; Gomperts, R.; Mennucci, B.; Hratchian, H. P.; Ortiz, J. V.; Izmaylov, A. F.; Sonnenberg, J. L.; Williams-Young, D.; Ding, F.; Lipparini, F.; Egidi, F.; Goings, J.; Peng, B.; Petrone, A.; Henderson, T.; Ranasinghe, D.; Zakrzewski, V. G.; Gao, J.; Rega, N.; Zheng, G.; Liang, W.; Hada, M.; Ehara, M.; Toyota, K.; Fukuda, R.; Hasegawa, J.; Ishida, M.; Nakajima, T.; Honda, Y.; Kitao, O.; Nakai, H.; Vreven, T.; Throssell, K.; Montgomery, J. A., Jr.; Peralta, J. E.; Ogliaro, F.; Bearpark, M. J.; Heyd, J. J.; Brothers, E. N.; Kudin, K. N.; Staroverov, V. N.; Keith, T. A.; Kobayashi, R.; Normand, J.; Raghavachari, K.; Rendell, A. P.; Burant, J. C.; Iyengar, S. S.; Tomasi, J.; Cossi, M.; Millam, J. M.; Klene, M.; Adamo, C.; Cammi, R.; Ochterski, J. W.; Martin, R. L.; Morokuma, K.; Farkas, O.; Foresman, J. B.; Fox, D. J. Gaussian, Inc., Wallingford CT, **2016**.

(24) Lee, C.; Yang, W.; Parr, R. G. Development of the Colle-Salvetti Correlation-Energy Formula into a Functional of the Electron Density. *Phys. Rev. B* **1988**, *37*, 785–789.

(25) Becke, A. D. Density-Functional Thermochemistry. III. The Role of Exact Exchange. *J. Chem. Phys.* **1993**, *98*, 5648–5652.

(26) Hay, P. J.; Wadt, W. R. Ab Initio Effective Core Potentials for Molecular Calculations. Potentials for K to Au Including the Outermost Core Orbitals. *J. Chem. Phys.* **1985**, *82*, 299–310.

(27) Hay, P. J.; Wadt, W. R. Ab Initio Effective Core Potentials for Molecular Calculations. Potentials for the Transition Metal Atoms Sc to Hg. *J. Chem. Phys.* **1985**, *82*, 270–283

(28) Hehre, W. J.; Ditchfield, K.; Pople, J. A. Self-Consistent Molecular Orbital Methods. XII. Further Extensions of Gaussian-Type Basis Sets for Use in Molecular Orbital Studies of Organic Molecules. *J. Chem. Phys.* **1972**, *56*, 2257–2261

(29) Reed, A. E.; Weinstock, R. B.; Weinhold, F. Natural Population Analysis. *J. Chem. Phys.* **1972**, *83*, 735–746.

(30) Durndell, L. J.; Parlett, C. M. A.; Hondow, N. S.; Isaacs, M. A.; Wilson, K.; Lee, A. F. Selectivity Control in Pt-Catalyzed Cinnamaldehyde Hydrogenation. *Sci. Rep*. **2015**, *5*, 9425.

(31) Dong, C.; Lian, C.; Hu, S.; Deng, Z.; Gong, J.; Li, M.; Liu, H.; Xing, M.; Zhang, J. Size-Dependent Activity and Selectivity of Carbon Dioxide Photocatalytic Reduction over Platinum Nanoparticles. *Nat. Commun.* **2018**, *9*, 1252.

(32) Lamberti, C.; Zecchina, A.; Groppo, E.; Bordiga, S. Probing the Surfaces of Heterogeneous Catalysts by in situ IR Spectroscopy. *Chem. Soc. Rev.* **2010**, *39*, 4951–5001.

(33) Vovk, E. I.; Kalinkin, A. V.; Smirnov, M. Y.; Klembovskii, I. O.; Bukhtiyarov, V. I. XPS Study of Stability and Reactivity of Oxidized Pt Nanoparticles Supported on TiO_2. *J. Phys. Chem. C* **2017**, *121*, 17297–17304.

(34) Hertl, W.; Hair, M. L. Adsorption of Water on Silica. *Nature* **1969**, *223*, 1150–1151.

(35) Sindorf, D. W.; Maciel, G. E. ^{29}Si CP/MAS NMR Studies of Methylchlorosilane Reactions on Silica Gel. *J. Am. Chem. Soc.* **1981**, *103*, 4263–4265.

(36) Whitford, C. L.; Stephenson, C. J.; Gómez-Gualdrón, D. A.; Hupp, J. T.; Farha, O. K.; Snurr, R. Q.; Stair, P. C. Elucidating the Nanoparticle-Metal Organic Framework Interface of Pt@ZIF-8 Catalysts. *J. Phys. Chem. C* **2017**, 121, 25079–25091.

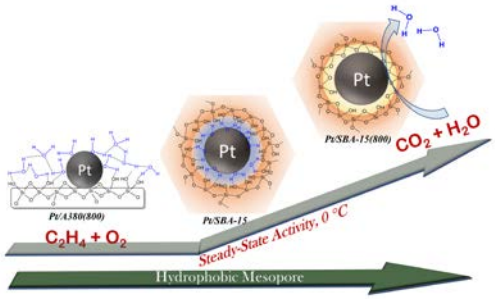
(37) Ding, K.; Gulec, A.; Johnson, A. M.; Schweitzer, N. M.; Stucky, G. D.; Marks, L. D.; Stair, P. C. Identification of Active Sites in CO Oxidation and Water-Gas Shift over Supported Pt Catalysts. *Science*. **2015**, *350*, 189–192.

(38) Brandt, R.; Hughes, M. R.; Bourget, L. P.; Truszkowska, K.; Greenler, R. The Interpretation of CO Adsorbed on Pt/SiO_2 of Two Different Particle-Size Distributions. Surf. Sci. Lett. **1993**, *286*, 15–25.

(39) Mihaylov, M.; Chakarova, K.; Hadjiivanov, K.; Marie, O.; Daturi, M. FTIR Spectroscopy Study of CO Adsorption on Pt-Na-Mordenite. *Langmuir* **2005**, *21*, 11821–11828.

(40) Avanesian, T.; Dai, S.; Kale, M. J.; Graham, G. W.; Pan, X.; Christopher, P. Quantitative and Atomic-Scale View of CO-Induced Pt Nanoparticle Surface Reconstruction at Saturation Coverage via DFT Calculations Coupled with in Situ TEM and IR. *J. Am. Chem. Soc*. **2017**, *139*, 4551–4558.

SYNOPSIS


Pt
Pt
Pt
Pt/A380(800)
Pt/SBA-15
Pt/SBA-15(800)
$CO_2 + H_2O$
$C_2H_4 + O_2$
Steady-State Activity, 0 °C
Hydrophobic Mesopore